Noninvasive identification of subcellular organization and nuclear morphology features associated with leukemic cells using light-scattering spectroscopy

Austin Hsiao
Martin Hunter
Cherry Greiner
Sharad Gupta
Irene Georgakoudi

Noninvasive identification of subcellular organization and nuclear morphology features associated with leukemic cells using light-scattering spectroscopy

Austin Hsiao,* **Martin Hunter, Cherry Greiner, Sharad Gupta,†** **and Irene Georgakoudi**
Tufts University, Biomedical Engineering Department, 4 Colby Street, Medford, Massachusetts 02115

Abstract. Leukemia is the most common and deadly cancer among children and one of the most prevalent cancers among adults. Improvements in its diagnosis and monitoring of leukemic patients could have a significant impact in their long-term treatment. We demonstrate that light-scattering spectroscopy (LSS)-based approaches could serve as a tool to achieve this goal. Specifically, we characterize the light scattering properties of leukemic (NALM-6) cells and compare them to those of normal lymphocytes and granulocytes in the 440–710 nm range, over ±4 deg about the exact backscattering direction. We find that the LSS spectra are well described by an inverse power-law wavelength dependence, with a power exponent insensitive to the scattering angle but significantly higher for leukemic cells than for normal leukocytes. This is consistent with differences in the subcellular morphology of these cells, detected in differential interference contrast images. Furthermore, the residual light-scattering signal, extracted after subtracting the inverse power-law fit from the data, can be analyzed assuming a Gaussian distribution of spherical scatterers using Mie theory. This analysis yields scatterer sizes that are consistent with the diameters of cell nuclei and allows the detection of the larger nuclei of NALM-6 cells compared to those of lymphocytes and granulocytes. © *2011 Society of Photo-Optical Instrumentation Engineers (SPIE)*. [DOI: 10.1117/1.3562925]

1 Introduction

Leukemia is a disorder of the bone marrow, where hematopoiesis (i.e., production of blood cells) takes place. It is expected to affect more than 44,000 adults and about 3,500 children under the age of 15 in the United States.[1,2] Although leukemia affects more adults than children, it is the most common pediatric cancer, representing 32% of all cancers for children younger than 15 years and 46% of malignancies among 2–4 year olds.[2] The most common childhood leukemia is acute lymphoblastic leukemia (ALL), affecting ∼80% of pediatric leukemia patients.[3] These malignancies involve transformation of a progenitor cell, which leads to dysregulated growth and arrested differentiation.[4] These progenitor cells or blasts are never found in the peripheral blood of a healthy person. However, at the time of leukemia diagnosis, blasts are usually present in peripheral blood and patients typically have elevated leukocyte counts. In fact, the initial leukocyte count was found to be a significant predictor of treatment outcome, with higher leukocyte counts corresponding to a worse prognosis.[3]

Treatment involves administration of a combination of chemotherapeutic agents and cranial radiation, and usually lasts 2–3 years.[3] The optimal duration of therapy remains unknown.

Detection of minimal residual disease (MRD) following treatment may play a significant role in determining the minimal duration of therapy required to achieve long-term remission, especially in children, where the long-term side effects of chemotherapy may be particularly detrimental to their physical and psychological development. The two most commonly used methods for detecting MRD include polymerase chain reaction (PCR)-based methods and flow cytometry. A number of studies have demonstrated that there is good correlation between the level of MRD and the probability of relapse,[5–9] even when the sensitivity is on the order of 2–5 cells in 1000.[10] One of the limitations of these methods is that the leukemic clones or the immunophenotype of leukemic cells may change during disease progression or treatment, leading to false-negative or false-positive results.[11–13] Sample contamination may also provide erroneous results. Most MRD studies examine cells from bone marrow aspirations or biopsies. However, MRD detection in the peripheral blood has also been shown to correlate well with relapse, occurring in 80% of patients with detectable MRD in the peripheral blood at the end of remission induction therapy, but only in 13% of patients with MRD confined to the bone marrow.[14] Therefore, improved methods of detecting leukemic cells within bone marrow aspirates or peripheral blood could significantly impact the detection and treatment of this disease, especially in pediatric patients.

Light-scattering spectroscopy (LSS)-based approaches could aid in the development of better or novel ways to diagnose and monitor leukemia. Such approaches have been shown capable of

*Currently at University of Illinois Urbana-Champaign, Bioengineering Department, 3120 Digital Computer Laboratory, MC-278, 1304 West Springfield Avenue, Urbana, Illinois 61801.
†Currently at University of California at Riverside, Bioengineering Department, Bourns Hall A217, Riverside, California 92521.

Address all correspondence to: Irene Georgakoudi, Biomedical Engineering Department, Tufts University, 4 Colby Street, Medford, Massachusetts 02115. Tel: 617-627-4353; Fax: 617-627-3231; E-mail: Irene.georgakoudi@tufts.edu

detecting subtle changes in the subcellular and nuclear organization and morphology of numerous types of cancer cells.[15–23] In addition, wavelength- and angle-dependent light-scattering measurements have been used to distinguish the different types of white blood cells.[24–29] Therefore, it is likely that LSS-based measurements could aid in the development of improved noninvasive or minimally invasive approaches to diagnose and monitor leukemic patients.

In this study, we characterize the light-scattering properties of NALM-6 ALL cells in the 440–710 nm range within the ±4-deg scattering angle range about the exact backscattering direction (i.e., we refer to the exact backscattering angle as 0 deg). We compare these measurements to light-scattering maps acquired from populations of normal lymphocytes and granulocytes, which are the two dominant populations of circulating white blood cells. To account for the dominant features of the observed light-scattering patterns from all cell populations, we employ a model that assumes an inverse–power-law dependence of the measured light scattering signal as a function of wavelength.

Furthermore, we find that the residual signal is in good agreement with Mie scattering from a sphere, whose size and refractive index are consistent with expected nuclear features of the different types of cells. This analysis reveals significant differences in the subcellular organization and nuclear features between leukemic and normal white blood cells and illustrates the potential of light-scattering-based methods as diagnostic tools for leukemia.

2 Material and Methods

2.1 Cell Culture

Established NALM-6 cells (DSMZ) were cultured in RPMI-1640, 1% penicillin/streptomycin, and 10% fetal bovine serum medium. The cells were kept in a sterile incubator and passaged every two days up to passage number 25. Peripheral blood was harvested from informed and consenting healthy adult men and women who ranged in age from 20 to 35 years old. To isolate the lymphocytes, harvested blood was layered over histopaque-1077 Sigma-Aldrich (St. Louis, MO) in 3:2 ratio and centrifuged at 1600 rpm for 20 min at room temperature. The centrifugation process separated the components of the blood according to their density, and the lymphocytes were recovered at the interface between blood and histopaque. The recovered lymphocytes were washed twice with RPMI-1640, 1% fetal bovine serum medium at 1600 rpm for 10 min. Isolation of granulocytes followed the same procedure described above using histopaque-1091 instead of 1077. The cells were enumerated using a hemacytometer, and the morphology of cells was examined under a light microscope using an oil immersion, 60X/1.4 NA objective. Next, the cells were suspended in 1.1 mL of RPMI-1640 with 1% penicillin/strepomycin in an Attofluor cell chamber Invitrogen (Carlsbad, CA). Before imaging, the cells in suspension were allowed to settle for 30 mins. The concentration of the cell suspension was 3×10^6 cells/ml in order to ensure a monolayer of cells.

2.2 LSS Measurements

The LSS system used in this study has been described in detail previously.[22] Briefly, the setup acquired the scattering angle- and wavelength-dependent intensity of light scattered in the backward direction. A collimated and linearly polarized light beam from a 500-W Xenon arc lamp was used for illuminating the sample at 45 deg from the surface normal to avoid detecting specular reflections. The backscattered light was detected through an analyzer that was placed either parallel (I_{par}) or perpendicular (I_{perp}) to the polarizer. The Fourier plane of the backscattered light was focused onto the entrance slit of a spectrograph, and LSS intensity maps were then collected on a CCD detector over the wavelength region $\lambda = 440$–710 nm, polar angle range $-4.2 < \theta < 4.2$ deg and azimuthal angle $\phi = 0$ deg. Polarization gating was used to facilitate interpretation of the LSS data with models based on single light scattering.[16–18,21,22] Singly scattered photons maintain their initial polarization, whereas multiply scattered photons are depolarized and consist of equal amounts of light polarized along the parallel and perpendicular polarizations. Thus, the differential LSS signal, $\Delta I = I_{par} - I_{perp}$ can be used to select only singly scattered light from a specimen. The acquisition time for each scattering map was 5 min. To account for angular and spectral system dependencies (e.g., lamp spectral variations, grating transmission, and CCD camera quantum efficiency), the background subtracted data were normalized using a scattering map acquired from a 99% reflectance standard (LabSphere).

2.3 LSS Data Analysis

At all polar angles, the residually polarized LSS spectra, $\Delta I(\lambda)$, were dominated by an inverse power-law wavelength dependence, $\Delta I(\lambda) \propto \lambda^{-\gamma}$. The power exponent, γ, was individually determined via linear least-squares fitting at several polar angles ($\theta = \pm 1$, ± 2, and ± 3 deg). The fit residuals were small [a few percent of the $\Delta I(\lambda)$ power-law component] and showed marked oscillations, which varied in frequency among normal and cancerous leukocytes. Mie theory was used to correlate the small oscillatory LSS component to leukocyte nuclear diameter.

A look-up table of Mie spectra was generated for comparison against our experimental LSS data, using the following range of scattering and particle parameters: particle diameter, d = 2–13 μm, in increments of $\Delta d = 0.05$ μm; standard deviation of diameter, $\sigma = 0.1$–1 μm, in increments of $\Delta\sigma = 0.01$ μm; particle refractive index, $n_{part} = 1.36$–1.45, in increments of $\Delta n_{part} = 0.005$; medium refractive index, $n_{med} = 1.36$; scattering angles $\theta = 179$ deg (1 deg backscattering) and $\phi = 0$ deg; wavelength $\lambda = 440$–710 nm. The Mie spectra were mean centered, and the best fit to the LSS data was selected by minimization of the Pearson product moment from all Mie spectra in the look-up table.

2.4 Differential Interference Contrast Microscopy Measurements

Differential interference contrast (DIC) microscopy images of lymphocytes, granulocytes, and acute lymphocytic leukemia cells (NALM-6) were obtained along with the LSS measurements. The diameter of lymphocyte and NALM-6 nuclei was measured using ImageJ and calibrated with the image of a staged graticule. For each cell population, at least 20 individual cells were measured from one DIC image. Possibly as a result of the actual morphology of granulocytes, the quality of DIC images we could obtain from this population was not high enough to
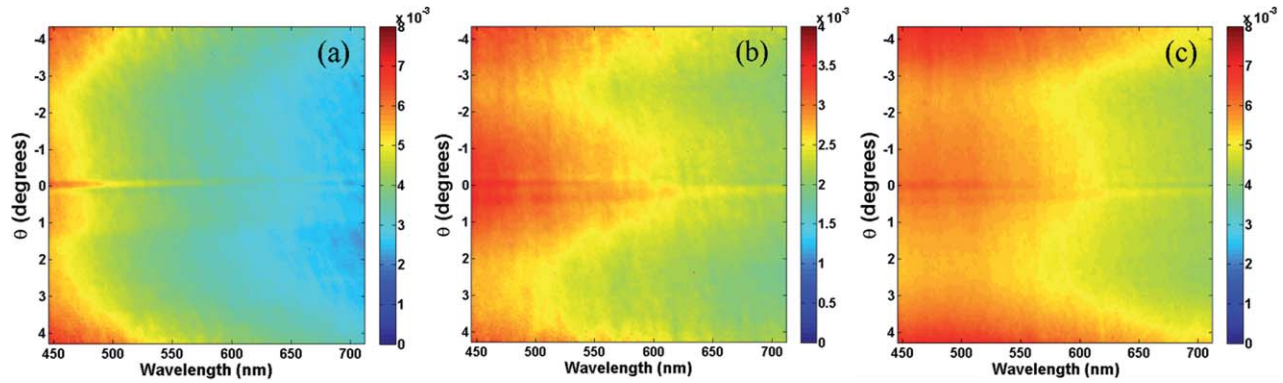
Fig. 1 Polarized LSS backscattering maps, $\Delta I(\lambda, \theta; \phi = 0$ deg$)$, from leukocyte cell monolayers: (a) NALM-6, (b) lymphocytes, and (c) granulocytes.

allow clear visualization of the nuclear lobes; thus, in this case, we relied on published estimates of these features.

Fourier analysis of the DIC images was used to characterize the subcellar morphology of the different leukocytes studied here. For each cell type, a 64×64 pixel intracellular region was selected from each of six randomly selected cells. The angularly averaged radial power spectral density (PSD) function, $\Phi(\kappa)$, was evaluated for each of these selected DIC regions as a function of radial spatial frequency, κ. The PSD spectra were found to consistently follow an inverse power-law dependence, $\Phi(\kappa) \propto \kappa^{-\beta}$, at intermediate values of spatial frequency ($0 < \log \kappa < 0.4\,\mu m^{-1}$ for lymphocytes and granulocytes, and $0 < \log \kappa < 0.3\,\mu m^{-1}$ for NALM-6 cells). The exponents β were evaluated by linear fitting of the PSD functions in log-log space over these intermediate ranges of κ. NALM-6 cells showed a clear trend toward higher values of β than normal leukocytes; the statistical significance of these differences was determined using analysis of variance (ANOVA) and t-test analyses.

3 Results

Differential LSS maps of all three leukocyte specimens revealed symmetry around the exact backscattering direction ($\theta = 0$ deg) and exhibited a smooth dependence on the wavelength. (Fig. 1). Representative spectra from each population at $\theta = 1$

deg are shown in Fig. 2(a). The corresponding fits of the inverse power-law wavelength-dependent expression to the data are also included and demonstrate excellent agreement. The inverse power-law exponent, γ, was relatively insensitive to scattering angle for each population [Fig. 2(c)]. However, significant differences in γ were observed between different leukocyte specimens (Fig. 2). For example, at $\theta = 1$ deg the LSS inverse power-law exponents were $\gamma = 0.86 \pm 0.10, 0.70 \pm 0.04$, and 1.83 ± 0.07 for lymphocytes, granulocytes, and NALM-6 specimens, respectively. In addition, the absolute backscattering cross section was found to be highest for granulocytes and lowest for lymphocytes [Fig. 2(a)]. Using a two-tailed t-test, the values of γ from NALM-6 cell specimens were found to be significantly higher ($p < 0.001$) compared to both lymphocyte and granulocyte populations. Small but statistically insignificant differences were observed in the γ values of granulocytes and lymphocytes. In Fig. 2(c), the exponent values of all three positive and negative θ angles revealed the said symmetry of the intensity map.

Residual LSS spectra were extracted by subtracting the inverse-power-law fits from the data. Representative residual spectra from each population along with corresponding fits achieved using a Mie theory–based model that assumes a Gaussian distribution of scatterers are included in Fig. 3. Fitting revealed the presence of a number of local minima. The global minima values were used to identify the best-fit parameter
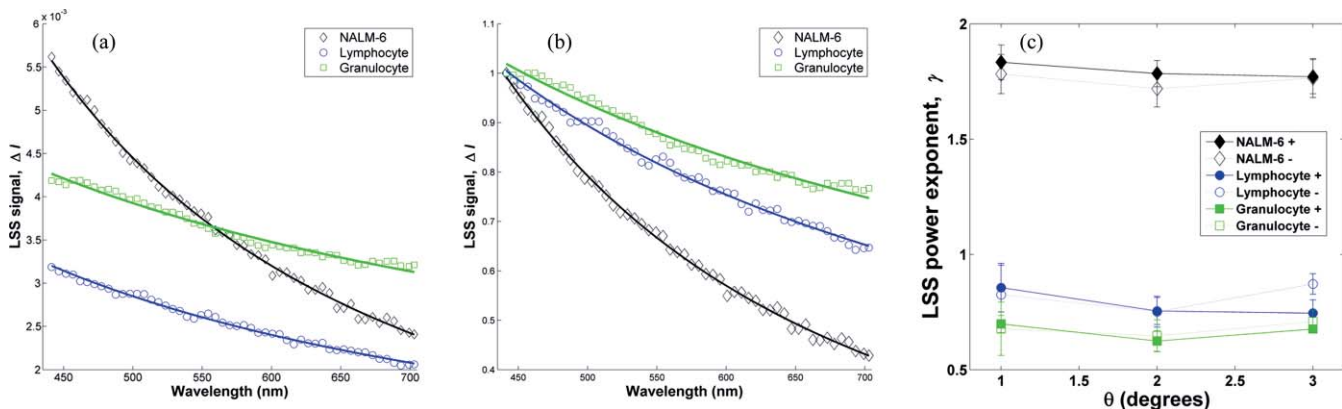
Fig. 2 (a) LSS spectra, $\Delta I(\lambda; \theta = 1$ deg, $\phi = 0$ deg$)$ from leukocyte monolayers. Solid lines are inverse power-law fits to the data. (b) Same as (a), but LSS spectra are intensity-normalized for comparison of relative spectral dependence. (c) Inverse power-law exponents, γ, obtained from fits to LSS spectra at six different backscattering angles: $\phi = 0$ deg, $\theta = \pm 1, \pm 2,$ and ± 3 deg. The sign of the polar scattering angle, θ, is indicated in the legend ($+$ or $-$).
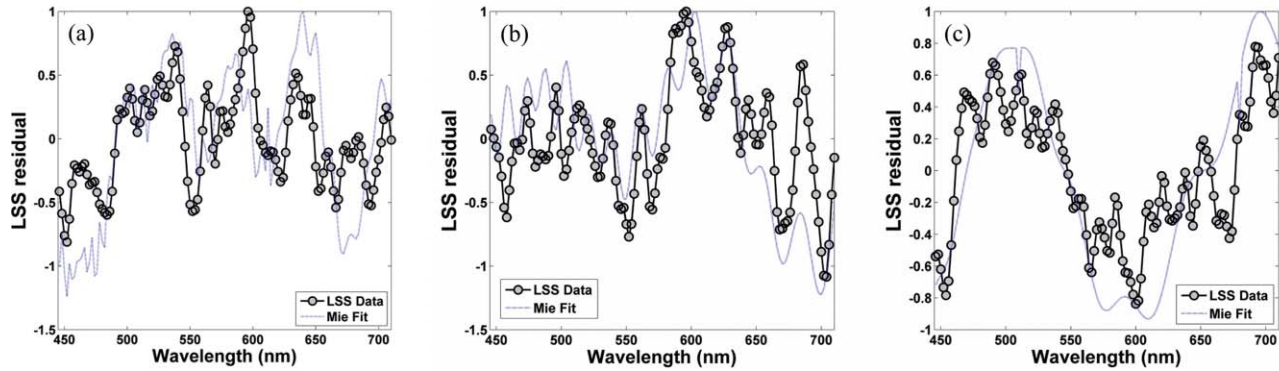
Fig. 3 Residuals of inverse power-law fits to LSS spectra at scattering angle $\theta = 1$ deg, $\phi = 0$ deg and Mie theory fits to the LSS residuals: (a) NALM-6, (b) lymphocytes, and (c) granulocytes.

values. Specifically, we achieved the best fits for the granulocytes when $d = 3$ μm and $\sigma = 0.11$ μm, for the lymphocytes when $d = 4.5$ μm and $\sigma = 0.38$ μm and for the NALM-6 cells when $d = 11.7$ μm and $\sigma = 0.49$ μm. Although the indices of refraction of the particles varied from one cell population to another, all the values were higher than the index of refraction of the surrounding medium. As shown in Table 1, there is generally good agreement between the nuclear diameter size acquired from our DIC measurements (Fig. 4) or other studies and the scattering particle diameters extracted from fitting of the residual LSS spectra. For the granulocytes, the reported diameter is consistent with the expected diameter of each one of the lobuli of the nucleus. The LSS extracted diameter for lymphocytes is lower than what we anticipate, and this error could be the result of particularly low signal-to-noise ratio because this population yielded the lowest overall scattering levels. For the NALM-6 cells, we achieve very good agreement with the DIC measurements we perform on our cell population. However, both the LSS and DIC extracted diameters are a little higher than previously reported values of the nucleus of NALM-6 cells acquired using fluorescence staining and confocal imaging.[29] This could be a result of the staining procedure or real differences in the morphology of the two NALM-6 populations.

Our DIC images were frequency analyzed to detect differences in the subcellular morphology of the various leukocyte populations. Figure 5 illustrates the result of Fourier analysis of the intracellular region of a randomly selected, DIC-imaged NALM-6 cell. An inverse power-law dependence of the radial PSD function, $\Phi(\kappa)$, evidenced by a linear regime in the log-log plot of $\Phi(\kappa)$ versus spatial frequency, κ, was a feature common to all leukocyte specimens (Fig. 6). The PSD inverse power-law exponents, β, for each cell type were obtained by averaging the β values determined from six randomly selected intracellular regions. The average values (± 1 standard deviation) of β thus obtained were 3.8 ± 0.4, 4.4 ± 0.4, and 5.0 ± 0.8 for granulocytes, lymphocytes, and NALM-6 cells, respectively. Figure 7 shows the correlation observed between these DIC PSD exponents and the inverse power-law exponent, γ, from the corresponding LSS spectra.

4 Discussion

Single backscattering LSS measurements in human and animal cells or tissues often show an inverse power-law spectral dependence.[18,21–23] The power exponent tends to vary significantly between normal and diseased (dysplastic or cancerous) cells, making LSS a promising optical technique for noninvasive clinical diagnoses. It is yet unclear, however, what exact morphological information is contained in these LSS spectra. The source of inverse power-law scattering contributions is generally accepted to be subcellular, submicron components, whose dimensions are either similar or substantially smaller than the wavelength of the scattered light. The most common approach has been to model these LSS spectra with Mie theory, assuming an ensemble of independent spherical, uniform scatterers with an inverse power-law size distribution, $N(d) \propto d^{-\beta}$. In these

Table 1 Summary of cellular nuclei parameter set for leukocytes from numerical comparison with Mie solution, DIC measurements and published literature (Ref. 5). (1) and (2) denote different patients. N/A denotes values that were not obtained due to unavailable data.

Sample	Mean diameter of cell nucleus (μm)			Standard deviation of diameter of cell nucleus (μm)		
	LSS	DIC	Literature	LSS	DIC	Literature
NALM-6	11.7	11.45	8.24[a]	0.49	1.22	N/A
Lymphocyte	4.5	6.65	(1) 6.4, (2) 6.3[b]	0.38	0.84	(1) 0.7, (2) 0.5[b]
Granulocyte	3.0	N/A	(1) 4.35, (2) 3.6[b]	0.11	N/A	(1) 0.65, (2) 0.55[b]

[a]Reference 27.
[b]Reference 18.
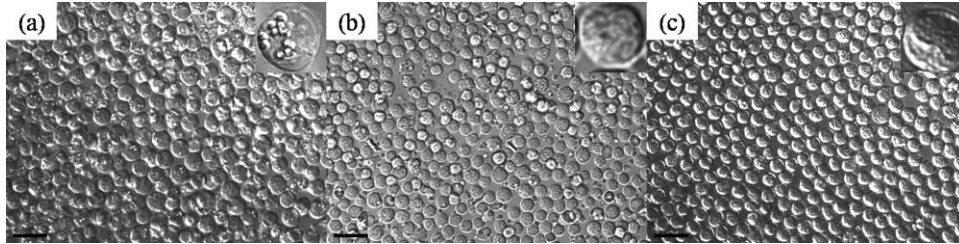
Fig. 4 DIC images of leukocyte cell monolayers: (a) NALM-6, (b) lymphocytes, and (c) granulocytes. Scale bar is 20 μm.
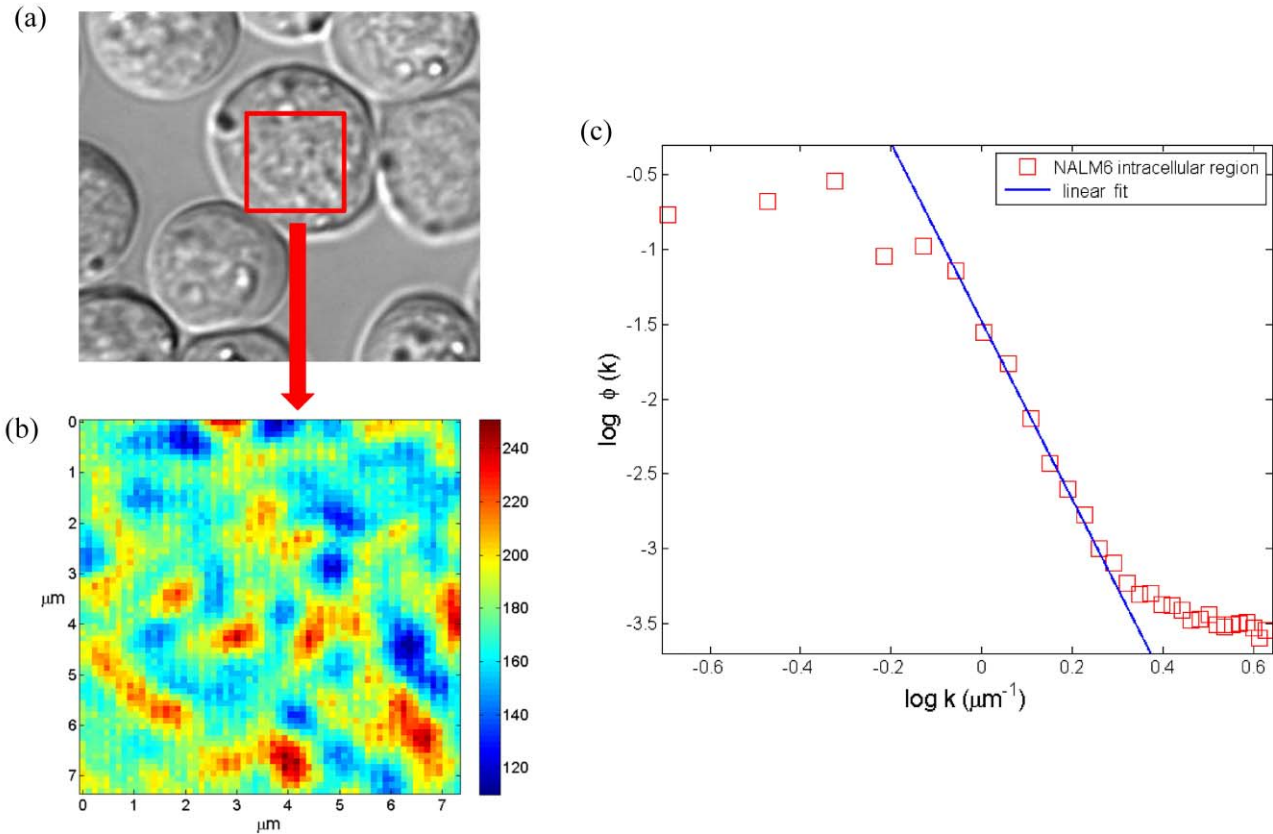
Fig. 5 Fourier analysis of NALM-6 DIC image: (a) DIC image of NALM-6 cell monolayer, (b) intracellular region (64×64 bins) randomly selected for Fourier analysis, and (c) log-log plot of PSD for selected NALM-6 intracellular region, with linear fit to inverse power-law regime.
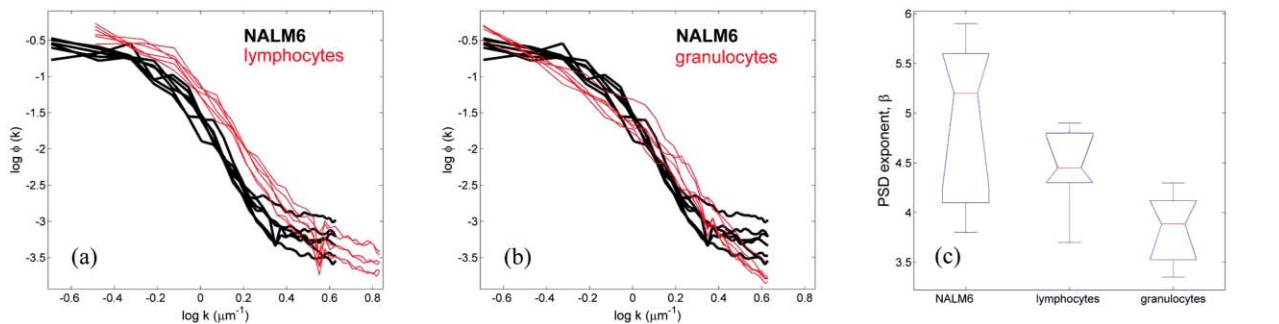
Fig. 6 Comparison of DIC PSD spectra for various leukocytes: (a) NALM-6 versus lymphocytes, (b) NALM-6 versus granulocytes, and (c) ANOVA plot for PSD power-law exponents, β, obtained from NALM-6 cells, lymphocytes, and granulocytes.
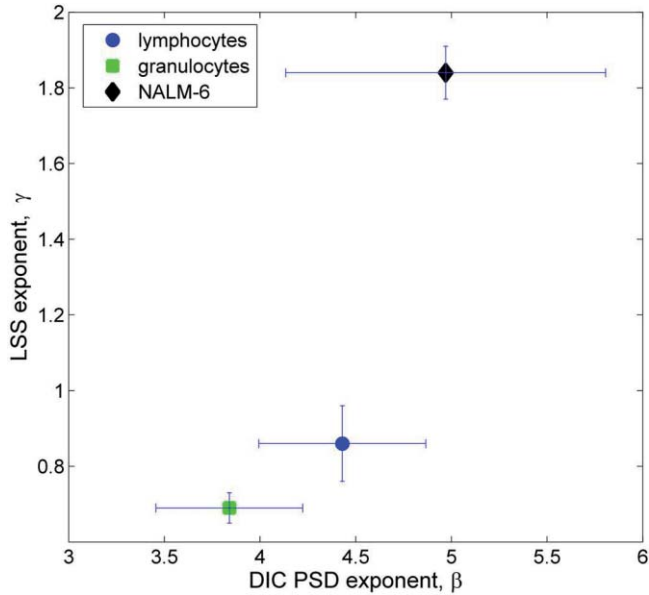
Fig. 7 Correlation of LSS power exponents, γ, with DIC PSD power exponents, β.

models, the typical range of particle diameters, d, required for optimal fit of power-law LSS spectra is 10 nm $< d <$ 2 μm.[18,22] However, despite successfully modeling the observed inverse power-law behavior of the LSS spectra, this approach vastly oversimplifies the complex intranuclear and cytoplasmic morphology of cells.

Several models have therefore been developed to more accurately describe the scattering of light from realistic subcellular inhomogeneities. A feature common to all these methods is the assumption of fractal organization of the continuous density fluctuations within tissues and cells, down to the nanometer scale.[19,21–23] In addition, these models make use of the first Born approximation[20] to derive analytical expressions for LSS spectra based on simple Fourier analysis techniques. Although some questions remain as to the applicability of the Born approximation at cellular length scales,[30] its relevance for scattering from submicron cellular features is justified by the low refractive index contrast of subcellular inhomogenities.

According to the Born approximation, our LSS spectra, $\Delta I(\lambda)$, are given by the Fourier transform of the tissue refractive index correlations, $C(\mathbf{r})$,[30]

$$\Delta I(\lambda) \propto \lambda^{-4} \int C(\mathbf{r}) \exp[i\mathbf{q} \cdot \mathbf{r}] \, d^3\mathbf{r}, \qquad (1)$$

where $C(\mathbf{r}) = \int [n^2(\mathbf{r}') - 1][n^2(\mathbf{r}' + \mathbf{r}) - 1] d^3\mathbf{r}'$, with $\mathbf{r}$ the vector correlation distance; $n(\mathbf{r})$ is the tissue refractive index; $\mathbf{q}$ is the scattering vector, with modulus $q = 2k \sin(\theta/2)$, wavevector $k = 2\pi/\lambda$ and polar scattering angle θ. It follows from Eq. (1) that if an LSS spectrum exhibits an inverse power-law spectral dependence, $\Delta I(\lambda) \propto \lambda^{-\gamma}$, then the scatterer refractive index correlations must also be a power law, $C(\mathbf{r}) \propto \mathbf{r}^{-\delta}$, with $\delta = \gamma - 1$. The scale invariance of such a correlation function is a defining characteristic of a fractal object.

Several interpretations of the autocorrelation power-law exponent, δ, have been proposed in the literature. The earliest approach associates δ with a mass fractal (self-similar) dimension,

D_M, of the density fluctuations of the scattering medium, via $D_M = 3 - \delta$.[19] In deriving this relationship, the authors make reference to the mass fractal organization of diffusion-limited aggregates and how it results in inverse power-law light-scattering spectra from these aggregates.[31] No attempt, however, is made to describe in what manner the subcellular density fluctuations organize themselves (if at all) as diffusion-limited aggregates. Mass fractal correlations may arise by other plausible mechanisms within cells. The crumpling of a uniform two-dimensional sheet,[32] for example, could be relevant to organelles with highly folded membrane structures. However, no direct evidence of such mass fractal structures within human cells and tissues have been reported.

Another modeling approach has been to assume continuously varying random fluctuations in the subcellular spatial refractive index, for which analytical solutions of the density autocorrelation function, $C(\mathbf{r})$, may be derived. All these approaches are based on a self-affine fractal organization of the subcellular inhomogeneities, akin to the von Karman density fluctuations observed in turbulent atmospheres.[33] Moscoso et al., for example, modeled the depolarization of light through biological tissue by assuming an exponential form of the tissue autocorrelation function—a special case of the more general von Karman autocorrelation.[34] Xu et al. later combined Moscoso's model with the Mie modeling approach, proposing a fractal tissue autocorrelation function consisting of an average of exponential functions weighted by an inverse power-law distribution of correlation lengths.[20] More recently, Hunter et al. published a generalized version of Moscoso's model in which the Born approximation was applied using the full von Karman autocorrelation function, rather than the special exponential case alone.[21]

Unlike the mass fractal models of light scattering by biological tissue, there is evidence in the published literature that biological cells and tissues do indeed exhibit self-affine morphologies. Self-affine fluctuations of tissue refractive index, for instance, have been observed at submicron scales by Schmitt and Kumar in normal human and mouse tissues by phase contrast microscopy.[33] Einstein et al. have also determined a self-affine organization of subnuclear chromatin in stained images of normal and malignant breast epithelial cell nuclei.[35] Autofluorescence images of mitochondrial nicotinamide adenine dinucleotide (NADH) in normal and precancerous engineered tissues have also shown a self-affine morphology at submicron scales.[36] The self-affine light-scattering models described above, however, are each limited in their own way, and their ultimate applicability to biological cells and tissue remains under question. The Moscoso model is based on a limiting case of the von Karman correlation function and is thus incapable of accounting for the full spectrum of possible self-affine fractal organization in biological specimens (with Hurst parameters ranging between the full range $0 < H < 1$). Xu's model has the additional complication of arbitrarily assuming an inverse power-law weighting of Moscoso exponential functions; furthermore, the physical interpretation of their derived fractal dimensions for various human tissues, with values $D > 4$, is unclear.

The fractal light scattering model proposed by Hunter et al.[21] adheres closest to the published evidence of self-affinity in human cells and tissue, and can consider the full range of allowed values of H for self-affine objects. Solution of the first Born

approximation [Eq. (1)] using the general von Karman autocorrelation function leads to the following dependence of the singly scattered light:

$$\Delta I(\lambda) \propto \lambda^{-4} \frac{1}{[1 + (4\pi L/\lambda)^2]^\alpha}, \qquad (2)$$

where the exponent α is related to the Hurst parameter, H, via H $= \alpha - D_E/2$, with D_E the Euclidian dimension of the scattering system, and L is the fractal upper scale (the upper bound of fractal correlation lengths).[21] The Hurst parameter is related to a self-affine object's fractal dimension, D, via $D = D_E + 1 - H$, and, as observed above, is limited to the range $0 < H < 1$.[37] For cases where the fractal upper scale is significantly larger than the wavelength of the scattered light, Eq. (2) reduces to a simple inverse power law, $\Delta I(\lambda) \propto \lambda^{2\alpha - 4}$, and might thus account for the inverse power-law dependence observed in our LSS spectra of leukocytes.

In its simplest application to biological cells, a value of $D_E = 3$ would be assumed in this model [i.e., a cell would be treated as a continuous 3-D body and its light scattering governed by its random (fractional Brownian) density fluctuations along all spatial directions]. In this case, LSS inverse power-law exponents would be expected to vary between $-1 < \gamma < 1$, depending on the value of the Hurst exponent, H, of the scattering object (cell). Our LSS spectra for normal leukocytes show power-law exponents in this allowed range, corresponding to values of H = 0.07 and 0.16 for lymphocytes and granulocytes, respectively. These values are consistent with previous determinations of Hurst parameters in other normal human cells and tissues,[35,36,38] whose values of H < 0.5 would indicate anticorrelated fractional Brownian organization of scatterer refractive index.[37]

The LSS inverse power-law exponents obtained from our NALM-6 cells, however, fall well outside the range allowed by this model ($\gamma = 1.84 \pm 0.07$). In previous work, Hunter et al.[21] argued that values of $D_E = 1$ or 2 could be invoked in LSS studies of cells and tissue, corresponding to filamentous or membranous structures that might dominate the light-scattering spectrum. There are two problems with that assumption, however. The first is that the structures would have to be unfolded (i.e., with strictly 1-D or 2-D embedding topologies), such as rigid rods or sheets, with the fractal density fluctuations constrained within them. It is conceivable that subcellular organelles, such as actin filaments and microtubules, may be well approximated by such a 1-D topology. However, typical membranous subcellular organelles are either highly folded structures or have a spherical shell geometry (e.g., lysozomes, nuclear membrane) of a length scale shorter than the coherence length of the detected scattered light ($>10 \mu$m for spectrometer resolutions <10 nm typical in these LSS experiments). Thus, unless spectrally unresolved white light is used in such LSS experiments to give coherence lengths of $<1 \mu$m; an assumption of $D_E = 2$ for light scattering from biological cells is unphysical. The other problem is that, even in the $D_E = 1$ case, the rigid filaments could be oriented at various polar and azimuthal angles relative to the incident-light polarization, and the LSS backscattering spectra would have to be modeled by averaging over all such 3-D orientations of the filaments. The problem is analogous to the 3-D diffraction of a plane wave from a tilted rectangular slit aperture (i.e., tilted at arbitrary polar and azimuthal angle relative to the incident plane wave vector). It has been shown that, in this case, a suitable

rotation of coordinate system still allows the scattering function to be evaluated via the traditional 2-D Fourier transform of the slit aperture.[39] This issue, however, has not been addressed in earlier work by Hunter et al.,[21] and must be tackled before consideration of $D_E = 1$ fractal scattering systems in their model.

The inability of the fractal scattering model proposed by Hunter et al.[21] to account for the inverse power-law LSS spectra from NALM-6 cells therefore remains unresolved. Future work examining the LSS spectra predicted from folded self-affine surfaces may shed insight into this problem. In addition, although the Born approximation has been verified to give good agreement with light-scattering data from single living cells,[40] application of more accurate models, such as the Rytov approximation, may provide a more accurate quantitative interpretation of LSS data from living cells.[38] Finally, a systematic increase in magnitude of our measured LSS power-law exponents could be arising from forward-scattering contamination. The experimental configuration used with a 45-deg angle of incidence of the excitation beam would suffice to eliminate forward-scattering contributions from clear samples. However, in turbid media such as biological cells, it is possible that a fraction of the mostly forward-scattered cone of light is reflected at the bottom glass surface and leads to detectable forward scattered light in our system. Mie theory calculations on inverse power-law distributions of spherical scatterers show a systematic increase in magnitude of the LSS inverse power-law exponent, when going from backward- to forward-scattering geometries. This effect may thus qualitatively account for the higher-than-expected LSS power exponent in NALM-6 cells (and possibly also in the normal leukocyte LSS data).

In light of these difficulties with previously reported fractal models of light scattering from biological cells, we restrict our current analysis to a qualitative interpretation of our LSS results. The scale invariance evidenced by the inverse power-law LSS spectra likely reflects some type of fractal subcellular morphology; however, its exact form (e.g., self-affine versus mass fractal geometry) cannot be inferred alone by our LSS experiments and would require more advanced methods, such as tomographic phase microscopy, for its direct elucidation.[38] Fourier analysis of our DIC images, however, provided semi-quantitative information on the subcellular morphology of our cells and corroborated the interpretation that changes in our LSS power-law exponents reflected changes in the subcellular morphology of our specimens.

It is well known that DIC image intensities are a highly nonlinear function of a scatterer's spatial density gradients.[41] Nevertheless, Figs. 5 and 6 indicate that spatial frequency analysis of our DIC images is valuable in quantitatively discerning leukemic cells from normal leukocytes. As observed in phase contrast microscopy images of human tissues,[33] as well as in autofluorescence images of normal and precancerous human keratinocytes,[36] Fourier analysis of our DIC images showed a scale-invariant, inverse power-law regime at submicron length scales. The PSD inverse power-law exponent, β, was significantly higher in NALM-6 cells (5.0 ± 0.8) than in granulocytes (3.8 ± 0.4); a two-tailed t-test of this dataset gave a p-value of 0.020. The difference in PSD exponent between NALM-6 and lymphocytes was less statistically significant (p-value of 0.21); however, Fig. 6(a) shows a significant shift in the PSD spectra of NALM-6 cells to lower spatial frequency compared to

lymphocytes. An ANOVA plot summarizing the statistical significance of our DIC data is given in Fig. 6(c). We also note that the DIC power-law exponents, β, are well correlated with the LSS power-law exponents, γ (Fig. 7), supporting the argument that backscattering LSS spectra from biological cells are dominated by their submicron subcellular morphology.

In conclusion, we demonstrate in this study that light-scattering spectroscopy can be used to reveal important differences in the subcellular organization and nuclear morphology of NALM-6 leukemic cells when compared to those of lymphocytes and granulocytes isolated from healthy individuals. Specifically, we show that, consistent with previous studies of epithelial cells[15–23] and our own DIC image analysis, the wavelength dependence of singly backscattered light from normal and cancerous white blood cells exhibits an inverse power-law behavior, which is consistent with fractal organization of subcellular scatterers whose sizes are in the submicron range. Importantly, we find that the exponent of this inverse power-law dependence is significantly higher for the leukemic cells compared to that for normal lymphocytes and granulocytes. Finally, we find that the residual light-scattering signal, which is not accounted by this model, is consistent with scattering from a Gaussian distribution of spherical scatterers described by Mie theory and corresponds to scattering particles with dimensions that are in agreement with those of cell nuclei. This latter analysis identifies significantly larger nuclei for the leukemic cells than the normal white blood cell populations that we consider. Therefore, simple LSS-based measurements have the potential to serve as useful tools in minimally invasive (e.g., lab-on-a-chip and fiber-optic-based systems) or noninvasive methods to improve on the sensitivity and specificity of detection of circulating leukemic cells.

References

1. "Leukemia classifications," <http://cancer.org> (13 May 2010).
2. L. A. Reis, M. A. Smith, J. G. Gurney, M. Linet, T. Tamra, J. L. Young, and G. R. Bunin, "Cancer incidence and survival among children and adolescents: United States SEER Program, 1975–1995," National Cancer Institute, SEER Program (1999).
3. M. Smith, D. Arthur, B. Camitta, A. J. Carroll, W. Crist, P. Gaynon, R. Gelber, N. Heerema, E. L. Korn, M. Link, S. Murphy, C. H. Pui, J. Pullen, G. Reamon, S. E. Sallan, H. Sather, J. Shuster, R. Simon, M. Trigg, D. Tubergen, F. Uckun, and R. Ungerleider, "Uniform approach to risk classification and treatment assignment for children with acute lymphoblastic leukemia," *J. Clin. Oncol.* **14**(1), 18–24 (1996).
4. R. Hoffman, E. Benz, S. Shattil, B. Furie, and H. Cohen, *Hematology: Basic Principles and Practice*, Churchill Livingstone, NY (2000).
5. C. Nyvold, H. O. Madsen, L. P. Ryder, J. Seyfarth, A. Svejgaard, N. Clausen, F. Wesenberg, O. G. Jonsson, E. Forestier, K. Schmiegelow, and Nordic Society for Pediatric Hematology and Oncology, "Precise quantification of minimal residual disease at day 29 allows identifica-

6. H. Cave, J. Van Der Werff ten Bosch, S. Suciu, C. Guidal, C. Waterkeyn, J. Otten, M. Bakkus, K. Thielemans, B. Grandchamp, and E. Vilmer, "Clinical significance of minimal residual disease in childhood acute lymphoblastic leukemia," *New Eng. J. Med.* **339**(9), 591–598 (1998).
7. M. J. Brisco, J. Condon, E. Hughes, S. H. Neoh, P. J. Sykes, R. Seshadri, I. Toogood, K. Waters, G. Tauro, and H. Ekert, "Outcome prediction in childhood acute lymphoblastic leukaemia by molecular quantification of residual disease at the end of induction," *Lancet* **343**(8891), 196–200 (1994).
8. C. J. Knechtli, N. J. Goulden, J. P. Hancock, V. L. Grandage, E. L. Harris, R. J. Garland, C. G. Jones, A. W. Rowbottom, L. P. Hunt, A. F. Green, E. Clarke, A. W. Lankester, J. M. Cornish, D. H. Pamphilon, C. G. Steward, and A. Oakhill, "Minimal residual disease status before allogeneic bone marrow transplantation is an important determinant of successful outcome for children and adolescents with acute lymphoblastic leukemia," *Blood* **92**(11), 4072–4079 (1998).
9. E. Coustan-Smith, F. G. Behm, J. Sanchez, J. M. Boyett, M. L. Hancock, S. C. Ralmondi, J. E. Rubnitz, G. K. Rivera, J. T. Sandlund, C. H. Pui, and D. Campana, "Immunological detection of minimal residual disease in children with acute lymphoblastic leukaemia," *Lancet* **351**(9102), 550–554 (1998).
10. J. F. San Miguel, A. Martinez, A. Macedo, M. B. Vidriales, C. López-Berges, M. González, D. Caballero, M. A. García-Marcos, F. Ramos, J. Fernández-Calvo, M. J. Calmuntia, J. Diaz-Mediavilla, and A. Orfao, "Immunophenotyping investigation of minimal residual disease is a useful approach for predicting relapse in acute myeloid leukemia patients," *Blood* **90**(6), 2465–2470 (1997).
11. A. M. Ford, K. Fasching, E. R. Panzer-Grumayer, M. Koenig, O. A. Haas, and M. F. Greaves, "Origins of "late" relapse in childhood acute lymphoblastic leukemia with TEL-AML1 fusion genes," *Blood* **98**(3), 558–564 (2001).
12. M. Konrad, M. Metzler, S. Panzer, I. Ostreicher, M. Peham, R. Repp, O. A. Haas, H. Gadner, and E. R. Panzer-Grumayer, "Late relapses evolve from slow-responding subclones in t(12;21)-positive acute lymphoblastic leukemia: evidence for the persistence of a preleukemic clone," *Blood* **101**(9), 3635–3640 (2003).
13. G. Janossy, F. J. Bollum, K. F. Bradstock, and J. Ashley, "Cellular phenotypes of normal and leukemic hemopoietic cells determined by analysis with selected antibody combinations," *Blood* **56**(3), 430–441 (1980).
14. E. Coustan-Smith, J. Sancho, M. L. Hancock, B. I. Razzouk, R. C. Ribeiro, G. K. Rivera, J. E. Rubnitz, J. T. Sandlund, C. H. Pui, and D. Campana, "Use of peripheral blood instead of bone marrow to monitor residual disease in children with acute lymphoblastic leukemia," *Blood* **100**(7), 2399–2402 (2002).
15. A. Brunsting, and P. F. Mullaney. "Differential light scattering from spherical mammalian cells," *Biophys. J.* **14**, 439–453 (1974).
16. J. R. Mourant, J. P. Freyer, A. H. Hielscher, A. A. Eick, D. Shen, and T. M. Johnson, "Mechanisms of light scattering from biological cells relevant to noninvasive optical-tissue diagnostics," *Appl. Opt.* **37**(16), 3586–3593 (1998).
17. V. Backman, R. Gurjar, and M. S. Feld. "Polarized light scattering spectroscopy for quantitative measurement of epithelial cellular structures *in situ*," *IEEE J. Sel. Top. Quantum Electron.* **5**(4), 1019–1026 (1999).
18. V. Backman, V. Gopal, and M. S. Feld. "Measuring cellular structure at submicrometer scale with light scattering spectroscopy," *IEEE J. Sel. Top. Quantum Electron.* **7**(6), 887–893 (2001).
19. A. Wax, C. Yang, V. Backman, K. Badizadeganm C. W. Boone, R. R. Dasari, and M. S. Feld, "Cellular organization and substructure measured using angle-resolved low-coherence interferometry," *Biophys. J.* **82**, 2256–2264 (2002).
20. M. Xu and R. R. Alfano, "Fractal mechanisms of light scattering in biological tissue and cells," *Opt. Lett.* **30**(22), 3051–3053 (2005).
21. M. Hunter, V. Backman, G. Popescu, M. Kalashnikov, C. W. Boone, A. Wax, V. Gopal, K. Badizadegan, G. D. Stoner, and M. S. Feld, "Tissue self-affinity and polarized light scattering in the Born approximation: a new model for precancer detection," *Phys. Rev. Lett.* **97**, 138102 (2006).
22. C. Mujat, C. Greiner, A. Baldwin, J. M. Levitt, F. Tian, L. A. Stucenski, M. Hunter, Y. L. Kim, V. Backman, M. Feld, K. Munger, and I. Georgakoudi, "Endogenous optical biomarkers of normal and human

papillomavirus immortalized epithelial cells," *Int. J. Cancer* **122**(2), 363–371 (2007).

23. C. S. Mulvey, C. A. Sherwood, and I. J. Bigio, "Wavelength-dependent backscattering measurements for quantitative real-time monitoring of apoptosis in living cells," *J. Biomed. Opt.* **14**(6), 064013 (2009).

24. V. Ost, J. Neukammer, and H. Rinneberg, "Flow cytometric differentiation of erythrocytes andleukocytes in dilute whole blood by light scattering," *Cytometry* **32**(3), 191–197 (1998).

25. G. I. Ruban, M. K. Sveltana, and D. V. Bockstaele. "Investigation of morphometric parameters for granulocytes and lymphocytes as applied to a solution of direct and inverse light-scattering problems," *J. Biomed. Opt.* **12**(4), 044017 (2007).

26. L. W. Terstappen, B. G. de Grooth, K. Visscher, F. A. van Kouterik, and J. Greve, "Four-parameter white blood cell differential counting based on light scattering measurements," *Cytometry* **9**(1), 39–43 (1988).

27. B. G. de Grooth, L. W. Terstappen, G. J. Puppels, and J. Greve, "Light-scattering polarization measurements as a new parameter in flow cytometry," *Cytometry* **8**(6), 539–544 (1987).

28. G. Otten and M. Loken, "Two color light scattering identifies physical differences between lymphocyte subpopulations," *Cytometry* **3**(3), 182–187 (1982).

29. R. S. Brock, X. Hu, D. A. Weidner, J. R. Mourant, and J. Q. Lu, "Effect of detailed cell structure on light scattering distribution: FDTD study of a B-cell with 3D structure constructed from confocal images," *J. Quant. Spectrosc. Radiat. Transfer* **102**, 25–36 (2006).

30. M. Born and E. Wolf, *Principles of Optics*, 7th ed., Cambridge University Press, Cambridge, England (1999).

31. J. Teixeira, "Experimental methods for studying fractal aggregates," in *On Growth and Form: Fractal and Non-Fractal Patterns in Physics*, H. E. Stanley and N. Ostrowsky, Eds., pp. 145–162, Nijhoff, Boston (1986).

32. M. A. Gomes, "Fractal geometry in crumpled paper balls," *Am. J. Phys.* **55**(7), 649–650 (1987).

33. J. M. Schmitt and G. Kumar, "Turbulent nature of refractive-index variations in biological tissue," *Opt. Lett.* **21**(16), 1310–1312 (1996).

34. M. Moscoso, J. B. Keller, and G. Papanicolau, "Depolarization and blurring of optical images by biological tissue," *J. Opt. Soc. Am. A* **18**(4), 948–960 (2001).

35. A. J. Einstein, H.-S. Wu, and J. Gil, "Self-affinity and lacunarity of chromatin texture in benign and malignant breast epithelial cell nuclei," *Phys. Rev. Lett.* **80**(2), 397–400 (1998).

36. J. M. Levitt, M. Hunter, C. Mujat, M. McLaughlin-Drubin, K. Munger, and I. Georgakoudi, "Diagnostic cellular organization features extracted from autofluorescence images," *Opt. Lett.* **32**(22), 3305–3307 (2007).

37. B. B. Mandelbrot, *The Fractal Geometry of Nature*, Rev ed., W. H. Freeman & Co., New York (2000).

38. M. Kalashnikov, W. Choi, C.-C. Yu, Y. Sung, R. R. Dasari, K. Badizadegan, and M. S. Feld, "Assessing light scattering of intracellular organelles in single intact living cells," *Opt. Express* **17**(22), 19674–19681 (2009).

39. H. J. Rabal, N. Bolognini, and E. E. Sicre, "Diffraction by a tilted aperture: coherent and partially coherent cases," *Opt. Acta* **32**(11), 1309–1311 (1985).

40. W. Choi, C.-C. Yu, C. Fang-Yen, K. Badizadegan, R. R. Dasari, and M. S. Feld, "Field-based angle-resolved light-scattering study of single live cells," *Opt. Lett.* **33**(14), 1596–1598 (2008).

41. S. V. King, A. Libertun, R. Piestun, C. J. Cogswell, and C. Preza, "Quantitative phase microscopy through differential interference imaging," *J. Biomed. Opt.* **13**, 024020 (2008).